Article:

Zhou, D., Pang, L.X., Wang, D.W. et al. (6 more authors) (2018) Crystal structure, impedance and broadband dielectric spectra of ordered scheelite-structured Bi(Sc1/3Mo2/3)O4 ceramic. Journal of the European Ceramic Society, 38 (4). pp. 1556-1561. ISSN 0955-2219

https://doi.org/10.1016/j.jeurceramsoc.2017.12.044

Crystal structure, impedance and broadband dielectric spectra of ordered scheelite-structured $Bi(Sc_{1/3}Mo_{2/3})O_4$ ceramic

Di Zhou*[a,b], Li-Xia Pang[a,c], Da-Wei Wang[a], Huan-Huan Guo,[b] FanYang[a], Ze-Ming Qi[d], Chun Li[e], Biao-Bing Jin[e] & Ian M. Reaney*[a]

[a]Department of Materials Science and Engineering, University of Sheffield, S1 3JD, UK

[b]Electronic Materials Research Laboratory, Key Laboratory of the Ministry of Education & International Center for Dielectric Research, Xi'an Jiaotong University, Xi'an 710049, Shaanxi, China

[c]Micro-optoelectronic Systems Laboratories, Xi'an Technological University, Xi'an 710032, Shaanxi, China

[e]National Synchrotron Radiation Laboratory, University of Science and Technology of China, Anhui, 230029, Hefei, China

[e]Research Institute of Superconductor Electronics (RISE), School of Electronic Science and Engineering, Nanjing University, Nanjing, Jiangsu, 210093, China.

Abstract

*Corresponding author E-mail address: zhoudi1220@gmail.com (Di Zhou) & i.m.reaney@sheffield.ac.uk (Ian M. Reaney)

$Bi(Sc_{1/3}Mo_{2/3})O_4$ ceramics were prepared via solid state reaction method. It crystallized with an ordered scheelite-related structure (a = 16.9821(9) Å, b = 11.6097(3) Å, c = 5.3099(3) Å and β = 104.649(2) °) with a space group C12/C1, in which Bi^{3+}, Sc^{3+} and Mo^{6+} are −8, −6 and −4 coordinated, respectively. $Bi(Sc_{1/3}Mo_{2/3})O_4$ ceramics were densifiedat 915 °C, giving a permittivity (ε_r) ~ 24.4, quality factor (Qf, Q=1/dielectric loss, f=resonant frequency) ~ 48,100 GHz and temperature coefficient of resonant frequency (TCF) ~ −68 ppm/°C. Impedance spectroscopy revealed that there was only a bulk response for conductivity with activation energy (E_a) ~ 0.97 eV, suggesting the compound is electrically and chemically homogeneous. Wide band dielectric spectra were employed to study the dielectric response of $Bi(Sc_{1/3}Mo_{2/3})O_4$ from 20 Hz to 30 THz. ε_r was stable from 20 Hz to the GHz region, in which only ionic and electron displacive polarization contributed to the ε_r.

Keywords: Microwave dielectric; $Bi(Sc_{1/3}Mo_{2/3})O_4$; low temperature co-fired ceramic (LTCC)

1. Introduction

Scheelite structured materials with a general formula ABO_4 have attracted much attention as photocatalysis and microwave dielectrics due to their adaptable structure which permits a wide range of solid solubility along with adjustable properties [1-8]. The scheelite-structure was first observed in the mineral, $CaWO_4$ and was named after its discoverer [9,10]. Scheelite typically has a tetragonal structure with space group, $I4_1/a$ (No. 88), in which the A- and B-cations are eight and four coordinated, respectively [1-8]. As summarized by Sleight and Linn [1], more than one hundred compounds have the scheelite structure with A cations ranging from A^+ (Li, Na, K, Ag, etc.), A^{2+} (Ca, Sr, Ba, etc.), A^{3+} (Bi, Ln, etc.) to A^{4+} (Zr, Hf, Ce, etc.), and B cations ranging from M^{3+} to M^{7+} (Ga, Fe, Ge, V, Nb, Mo, W, Re, I and Os) [1,11-14]. Nitrogen and fluorine can also partially substitute for oxygen [15]. Defects on the A site and complex cations occupying A and B sites usually lead to ordering and related monoclinic variants. A and B site ordered scheelite structures were first observed in $(K_{0.5}Eu_{0.5})MoO_4$ and $Bi(Fe_{1/3}Mo_{2/3})O_4$ [16,17]. Microwave dielectric properties of the scheelite-structured materials were first reported for Ca, Sr and Ba molybdates and tungstates [18,19] with high quality factor (Qf ~ 60,000 GHz) but low permittivity (ε_r < 12). Bismuth normally possesses a large ionic polarizability (α) and Bi-containing microwave dielectrics usually have large resulting ε_r. [20,21] When Bi cations fully occupy the A site in the scheelite structure, the B site is pentavalent (e.g V^{5+}) [1,22]. Pure $BiVO_4$ crystallizes in a monoclinic scheelite structure with a = 5.1956 Å > b = 5.0935 Å) and γ = 90.38 °) [23]. Although $BiVO_4$ possesses a high ε_r (~ 68), its Qf is only 8,000 GHz and its temperature coefficient of resonant frequency (TCF) ~ − 260 ppm/°C due to a ferroelastic phase transition at 255 °C [24,25]. B-site order through introducing complex ions such as $(Fe_{1/3}Mo_{2/3})^{5+}$ and $(In_{1/3}Mo_{2/3})^{5+}$, is an effective method to improve Qf as reported in our previous work [26,27]. In the present work, the sintering behavior, crystal structure, microstructure, impedance and dielectric spectra of the $Bi(Sc_{1/3}Mo_{2/3})O_4$ ceramics were studied.

2. Experimental Section

Sample Synthesis. Proportionate amounts of reagent-grade starting materials of Bi_2O_3 (> 99%, Sigma-Aldrich), Sc_2O_3 and MoO_3 (> 99%, Fisher Scientific) were measured according to the stoichiometric formulation $Bi(Sc_{1/3}Mo_{2/3})O_4$. Powders were mixed and ball-milled for 24 h using isopropanol. The powder mixture was then dried and calcined at 800 ^oC for 4 h. The calcined powders were re-milled for 24 h and pressed into cylinders (13 mm in diameter and 4 ~ 5 mm in height) at 50 MPa. Samples were sintered 2 h at 890 ^oC ~ 930 ^oC.

Structural and Microstructural Characterisation. X-ray diffraction (XRD) was performed using with CuKα radiation (Bruker D2 Phaser) form 5-80 ^{o} 2θ at a step size of 0.02 ^{o}. The results were analyzed by the Rietveld profile refinement method, using FULLPROF program. The structure was further investigated in transmission electron microscopy (TEM) using a JEOL 2100 transmission electron microscope operated at 200 kV. As-fired and fractured surfaces were observed by using a scanning electron microscopy (SEM, FEI, Inspect F).

Infrared Reflectivity, THz Transmission Measurement and Classical Oscillator Analysis. Room temperature infrared reflectivity spectra were measured using a Bruker IFS 66v FTIR spectrometer on Infrared beamline station (U4) at National Synchrotron Radiation Lab. (NSRL), China. The polished ceramic samples with flatness around 1μm were placed in a vacuum chamber at 2 mbar, and the reflectivity was obtained as the intensity relative to the reflectance of an evaporated gold mirror. The far and middle infrared spectra agreed well with each other in the overlapped frequency range. IR reflectivity spectra were analyzed by using a classical harmonic oscillator model as follows [28, 29]:

$$\varepsilon^*(\omega) = \varepsilon_\infty + \sum_{\mathrm{j}=1}^{\mathrm{n}} \frac{\omega_{\mathrm{pj}}^2}{\omega_{\mathrm{oj}}^2 - \omega^2 - \mathrm{j}\gamma_{\mathrm{j}}\omega}, \quad (1)$$

where $\varepsilon^*(\omega)$ is complex dielectric function, ε_∞ is the dielectric constant caused by the electronic polarization at high frequencies, γ_j, ω_{oj} and ω_{pj} are the damping factor, transverse frequency, and plasma frequency of the j-th Lorentz oscillator, respectively, and n is the number of transverse phonon modes. The relation between complex reflectivity $R^*(\omega)$ and permittivity $\varepsilon^*(\omega)$ can be written as:

$$\mathrm{R}^*(\omega) = \left| \frac{1-\sqrt{\varepsilon^*(\omega)}}{1+\sqrt{\varepsilon^*(\omega)}} \right|^2, \quad (2)$$

Based on well fitting, tt microwave region ($\omega \ll \omega pj$), hence, real part and imaginary part of microwave dielectric permittivity can be derived from equation (3):

$$\varepsilon'(\omega) = \varepsilon_\infty + \sum_{\mathrm{j}=1}^{\mathrm{n}} \frac{\omega_{\mathrm{pj}}^2}{\omega_{\mathrm{oj}}^2} = \varepsilon_\infty + \sum_{\mathrm{j}=1}^{\mathrm{n}} \Delta\varepsilon_{\mathrm{j}}, \quad (3)$$

$$\varepsilon''(\omega) = \omega \sum_{\mathrm{j}=1}^{\mathrm{n}} \frac{\Delta\varepsilon_{\mathrm{j}}\gamma_{\mathrm{j}}}{\omega_{\mathrm{oj}}^2}, \quad (4)$$

The dielectric behaviors over 0.2 to 1.2 THz (6.7 - 40 cm^{-1}) were measured by a terahertz time-domain (THz TDS) spectroscopy (ADVAVTEST TAS7500SP, Japan). A passive mode-lock fiber laser is used to pump and gate respectively two GaAs photoconductive antennas for the generation and detection of THz wave. The transfer function at THz region can be written as following [30-32]:

$$H^*(\omega) = \frac{E^*_{sam}(\omega)}{E^*_{ref}(\omega)}$$
$$= \frac{4n^*(\omega)}{(n^*(\omega))^2} \bullet \exp[-i\frac{(n^*(\omega)-1)\omega d}{c}] \times \left\{1+[\frac{n^*(\omega)-1}{n^*(\omega)+1}\exp(-i \bullet n^*(\omega)d/c)]^2\right\} \quad (5)$$

where, $E^*_{sam}(\omega)$ and $E^*_{ref}(\omega)$ are the recorded reference and sample signals, respectively. $n^*(\omega)$ is complex refractivity; d is thickness of sample; ω is angular frequency; c is the speed of light in vacuum. Then, complex permittivity $\varepsilon^*(\omega)$ can be obtained using the relation between complex refractivity $n^*(\omega)$ and complex permittivity $\varepsilon^*(\omega)$:

$$\sqrt{\varepsilon^*(\omega)} = n^*(\omega) \quad (6)$$

Impedance and Low Frequency Dielectric Property Measurements. Impedance spectroscopy measurements were performed on sintered ceramics coated with fired on Au-paste electrodes using a LCR (Agilent E4980A) and homemade heating system over 10^2–10^6 Hz from 350 to 600 °C. Room temperature ε_r and loss can be collected over 10^2–10^6 Hz.

Microwave Dielectric Property Measurement. Dielectric properties at microwave frequency were measured with the $TE_{01\delta}$ dielectric resonator method [33] with a network analyzer (Advantest R3767CH; Advantest, Tokyo, Japan) and a home-made heating system. The temperature coefficient of resonant frequency TCF (τ_f) was calculated with the following formula:

$$TCF(\tau_f) = \frac{f_{85} - f_{25}}{f_{25} \times (85-25)} \times 10^6 \quad (7)$$

where f_{85} and f_{25} are the $TE_{01\delta}$ resonant frequencies at 85 °C and 25 °C, respectively.

3. Results and Discussions

Crystal Structure, Coordination and Bonding.

$Bi(Sc_{1/3}Mo_{2/3})O_4$ ceramics crystallize in a B-site ordered scheelite structure. Experimental and calculated XRD profiles of the $Bi(Sc_{1/3}Mo_{2/3})O_4$ sample at room temperature are shown in Figure 1a in which a = 16.9821(9) Å, b = 11.6097(3) Å, c = 5.3099(3) Å and β = 104.649(2) ^{o} (R_p=9.03 %, R_{wp}=13.1 %, R_{exp}=12.8 % and the goodness of fit is defined as S= R_{wp} / R_{exp} = 1.02). The space group is C12/C1 (No. 15), which agrees well with previous reports [13]. For $Bi(Fe_{1/3}Mo_{2/3})O_4$, FeO_4 and MoO_4 tetrahedra are ordered [17] despite Fe^{3+} having a similar ionic radius (~ 0.49 Å) to Mo^{6+} (0.41 Å). In contrast, Sc^{3+} has much larger ionic radius than that of Fe^{3+} and Mo^{6+} and does not reside in tetrahedral coordination. As reported by Kolitsch and Tillmanns [13], Sc^{3+} prefers to be surrounded by six oxygens within a slightly distorted octahedron. The refined atomic fractional coordinates from XRD data and bond length data are listed in Table 1 and Table 2, respectively. Sc-O bond lengths are much larger than that of Mo-O but smaller than Bi-O [13]. A schematic of the crystal structure is illustrated in Figure 1b. Figure 1c shows the SAED patterns (inset) and high resolution images of $Bi(Sc_{1/3}Mo_{2/3})O_4$ viewed along the [13−2] zone axes. The rhombus pattern is composed of four O1 atoms with an internal angle of 75.8 ^{o}, similar to the refined value ~76.3 ^{o} from XRD patterns. In addition, the interplanar spacing of the O1 ions is measured from high resolution data as 0.491 and 0.478 nm which correspond well with XRD refinements.

Microstructure analysis.

SEM images of the as-sintered and fractured surfaces of a $Bi(Sc_{1/3}Mo_{2/3})O_4$ ceramic sintered 2h at 930^{o}C is shown in Figure 2. A dense homogeneous microstructure is observed consistent with a high relative density (96.7%) with the theoretical and apparent density, 6.968 g/cm^3 and 6.74 g/cm^3, respectively. Fracture surfaces, as shown in Figure 2b, of $Bi(Sc_{1/3}Mo_{2/3})O_4$ ceramics exhibited a mixture of transgranular and intergranular fracture, grain boundaries free from apparent second phase and a grain size ~ 1 to 3 μm.

Impedance analysis:

Complex impedance plane, Z^*, plots of $Bi(Sc_{1/3}Mo_{2/3})O_4$ ceramic at 448 and 502 °C are shown in Figure 3a. $Bi(Sc_{1/3}Mo_{2/3})O_4$ ceramics exhibited a single semicircular arc over the measured frequency range (20 Hz ~ 1 MHz) with an associated resistivity (R_b) of ~ 0.55 MΩ·cm and 1.52 MΩ·cm at 502 and 448 °C, respectively, which resulted from a bulk response with no grain boundary contribution. To confirm this observation, impedance data at different temperatures was fitted using a simple R-CPE model in parallel. The simulation parameters also indicated that within the frequency range (20 Hz ~ 1 MHz), contribution from the grain boundaries (defects) was negligible, which means that grain boundaries here might be electrically conductive. An Arrhenius plot of the temperature dependence of the bulk conductivity, σ ($1/R_b$), is shown in Figure 3b which gives an activation energy, E_a ~ 0.97 eV for bulk conduction, which indicated that the $Bi(Sc_{1/3}Mo_{2/3})O_4$ ceramic is a quite good insulating material.

Microwave dielectric properties.

ε_r and Qf of the $Bi(Sc_{1/3}Mo_{2/3})O_4$ ceramics as a function of sintering temperature are shown in Figure 4. ε_r increased from ~ 20 to a saturated value ~ 24.4 as sintering temperature increased from 890 °C to 930 °C due to the elimination of pores. Qf adopted a similar trend versus with ~ 48,100 GHz at 910 and 915 °C. As suggested by Shannon, the molecular polarizabilities of $Bi(Sc_{1/3}Mo_{2/3})O_4$ can be calculated according to:

$$\alpha_{Bi(Sc_{1/3}Mo_{2/3})O_4} = \alpha_{Bi^{3+}} + 1/3\alpha_{Sc^{3+}} + 2/3\alpha_{Mo^{6+}} + 4\alpha_{O^{2-}} \approx 17.28\,Å^3, \quad (8)$$

where the ionic polarizabilities of Bi^{3+}, Sc^{3+}, Mo^{6+} and O^{2-} were 6.12 $Å^3$, 2.81 $Å^3$, 3.28 $Å^3$ and 2.01 $Å^3$, respectively [18,34] Considering the Clausius–Mosotti relation [35]:

$$\varepsilon_{meas} = \frac{3V + 8\pi\alpha}{3V - 4\pi\alpha} \Rightarrow \alpha = \frac{3V(\varepsilon - 1)}{4\pi(\varepsilon + 2)} \approx 17.75\,Å^3, \quad (9)$$

where the V is the cell volume, 1006.42/12 = 83.868 $Å^3$, the measured molecular polarizability is about 17.75 $Å^3$ with an acceptable deviation about ~ 3 % from the calculated value. The sintering temperatures and microwave dielectric properties of low temperature firing microwave dielectric ceramics with permittivity value around ~ 25 are listed in Table 3 [36-41]. In fact, the commercial K25 materials used for dielectric resonators are mainly $Ba(Mg_{1/3}Ta_{2/3})O_3$ based ones [42], which usually possess an extreme high Qf value > 100,000 GHz and high sintering temperature about 1600 ^oC, and not suitable for LTCC technology. Compared with the similar scheelite structured $Bi(Fe_{1/3}Mo_{2/3})O_4$ and $Bi(In_{1/3}Mo_{2/3})O_4$, the $Bi(Sc_{1/3}Mo_{2/3})O_4$ ceramic possesses a higher Qf value. However, the TCF values of this series must be adjusted to near zero by solid solution or composite methods before they can be employed in applications. The $(A_{0.5}Bi_{0.5})MoO_4$ (A = Li, Na, K and Ag) materials with high positive TCF values might be good candidates to compensate the TCF of $Bi(Sc_{1/3}Mo_{2/3})O_4$ ceramic.

Infrared Reflectivity and THz Transmission Spectrum Study.

Wideband complex dielectric spectra of the $Bi(Sc_{1/3}Mo_{2/3})O_4$ ceramics in the frequency range 20 Hz ~ 30 THz and room temperature infrared reflectivity spectra are shown in Figure 5. ε_r at 20 Hz ~ 1 MHz was measured using an LCR meter and was stable at ~ 25, suggesting only a limited space charge contribution to polarization. The dielectric loss ($\varepsilon''/\varepsilon'$) from 20 Hz ~ 1 MHz was ~ 1×10^{-4}. ε_r at 6.84 GHz measured using a network analyzer and metal cavity was 24.4, close to the value recorded at lower frequencies, indicating no significant dipolar contribution to polarization from 20 Hz to the GHz region. The dielectric loss at 6.84 GHz was ~1.4×10^{-4}, slightly larger than that at lower frequencies whilst Qf was 48,100 GHz, high enough to be considered useful for resonator applications. In the THz region (0.1 ~ 1.4 THz), ε_r initially increased slightly but then sharply when entering the far-infrared range due photon absorption at ~ 65.383 cm^{-1}. As suggested by equation (4), the imaginary part of ε_r at THz increased almost linearly with frequency. As shown in Figure 5, the room temperature infrared reflectivity spectra may be fitted using 24 Lorentz modes as listed in Table 4. ε_r at optical frequencies is 2.72 and the fitted complex microwave permittivity using equation (3) and (4) is ~ 21.334 and 0.00342, close to measured values. Besides, the smaller fitted imaginary value of permittivity also shows some space of improvement for Qf value of the $Bi(Sc_{1/3}Mo_{2/3})O_4$ ceramic by fine processing in the future.

4. Conclusions

The $Bi(Sc_{1/3}Mo_{2/3})O_4$ ceramic densified at ≥ 915 °C with grain size 1 to 3 μm. The compound crystallized in an ordered scheelite structure with ~ a = 16.9821(9) Å, b = 11.6097(3) Å, c = 5.3099(3) Å and β = 104.649(2) ° with a space group C12/C1 (No. 15). Optimum microwave dielectric properties with a ε_r ~ 24.4 and Qf ~ 48,100 GHz were obtained for ceramics sintered 2h at 915 °C. Impedance spectra revealed only bulk conduction with an activation energy ~ 0.97 eV. Wideband dielectric spectra over 20 Hz to 30 THz indicated that the $Bi(Sc_{1/3}Mo_{2/3})O_4$ ceramic is a good insulator with low dielectric loss that night have potential for high frequency capacitor applications. We note however, that Sc_2O_3 and MoO_3 are comparatively expensive raw materials which might limit its commercial uptake.

Acknowledgements

This work was supported by Sustainability and Substitution of Functional Materials and Devices EPSRC (EP/L017563/1), the National Natural Science Foundation of China (U1632146), the Young Star Project of Science and Technology of Shaanxi Province (2016KJXX-34), the Key Basic Research Program of Shaanxi Province (2017GY-129), the Fundamental Research Funds for the Central University, and the 111 Project of China (B14040).

Reference

[1] A. W. Sleight, W. J. Linn, Olefin oxide over oxide catalysts with the scheelite structure, Ann. N. Y. Acad. Sci. 272 (1976) 22–44.

[2] A. W. Sleight, K. Aykan, D. B. Rogers, New Nonstoichiometric Molybdate, Tungstate, and Vanadate Catalysts with the Scheelite-Type Structure, J. Solid State Chem. 13 (1975) 231–236.

[3] J. Varghese, T. Siponkoski, M. Teirikangas, M. T. Sebastian, A. Uusimäki, H. Jantunen, Structural, Dielectric, and Thermal Properties of Pb Free Molybdate Based Ultralow Temperature Glass, ACS Sustainable Chem. Eng. 4 (2016) 3897–3904.

[4] N. Joseph, J. Varghese, T. Siponkoski, M. Teirikangas, M. T. Sebastian, H. Jantunen, Glass-Free $CuMoO_4$ Ceramic with Excellent Dielectric and Thermal Properties for Ultralow Temperature Cofired Ceramic Applications. ACS Sustainable Chem. Eng. 4 (2016) 5632–5639.

[5] M. T. Sebastian, H. Wang, H. Jantunena, Low temperature co-fired ceramics with ultra-low sintering temperature: A review, Curr. Opin. Solid State Mater. Sci. 20 (2016) 151-170.

[6] D. Zhou, C. A. Randall, L. X. Pang, H. Wang, J. Guo, G. Q. Zhang, Y. Wu, K. T. Guo, L. Shui, X. Yao, Microwave dielectric properties of $(ABi)_{1/2}MoO_4$ (A = Li, Na, K, Rb, Ag) type ceramics with ultra-low firing temperatures, Mater. Chem. Phys. 129 (2011) 688–692.

[7] L. X. Pang, D. Zhou, Z. M. Qi, W. G. Liu, Z. X. Yue, I. M. Reaney, Structure–Property Relationships of Low Sintering Temperature Scheelite-Structured (1-x)$BiVO_4$–x$LaNbO_4$ Microwave Dielectric Ceramics, J. Mater. Chem. C 5 (2017) 2695–2701.

[8] H. Kato, N. Matsudo, A. Kudo, Photophysical and Photocatalytic Properties of Molybdates and Tungstates with a Scheelite Structure, Chem. Let. 33 (2004) 1216–1217.

[9] R. M. Hazen, L. W. Finger, J. W. E. Mariathasan, High-pressure Crystal Chemistry of Scheelite-type Tungstates and Molybdates, J. Phys. Chem. Solids 46 (1985) 253–263.

[10] Klein, Cornelis and Cornelius S. Hurlbut, Manual of Mineralogy, Wiley, 20th ed., 1985, 356, ISBN 0-471-80580-7

[11] S. Tokunaga, H. Kato, A. Kudo, Selective preparation of monoclinic and tetragonal $BiVO_4$ with scheelite structure and their photocatalytic properties, Chem. Mater. 13 (2001) 4624–4628.

[12] J. W. E. Mariathasan, R. M. Hazen, L. W. Finger, High-pressure crystal chemistry of scheelite-type tungstates and molybdates, J. Phys. Chem. Solids 46 (1985) 253–263.

[13] U. Kolitsch, E. Tillmanns, $Bi_3ScMo_2O_{12}$: the difference from $Bi_3FeMo_2O_{12}$. Acta Crystallogr. E Struct. Rep. 59 (2003) i43–i46.

[14] P. Tarte, M. Liegeois-Duyckaerts, Vibrational studies of molybdates, tungstates and related compounds—I: New infrared data and assignments for the scheelite-type compounds $XIIMoO_4$ and $XIIWO_4$, Spectrochim. Acta Part A 28 (1972) 2029–2036.

[15] F. Cheviré, F. Tessier, R. Marchand, New scheelite-type oxynitrides in systems RWO_3N–AWO_4 (R= rare-earth element; A= Ca, Sr) from precursors obtained by the citrate route, Mater. Res. Bul. 39 (2004) 1091–1101.

[16] R. F. Klevtsova, L. P. Kozeeva, P. V. Klevtsov, Production and structure of Potassium-Duropium Molybdate Crystals $KEu(MoO_4)_2$, Kristallogr. 19 (1974) 89–94.

[17] A. W. Sleight, W. Jeitschko, $Bi_3(FeO_4)(MoO_4)_2$ and $Bi_3(GaO_4)(MoO_4)_2$ - new

compounds with scheelite related structures, Mater. Res. Bull. 9 (1974) 951–954.

[18] G. K. Choi, J. R. Kim, S. H. Yoon, K. S. Hong, Microwave dielectric properties of scheelite (A= Ca, Sr, Ba) and wolframite (A= Mg, Zn, Mn) $AMoO_4$ compounds, J. Eur. Ceram. Soc. 27 (2007) 3063–3067.

[19] S. H. Yoon, D. W. Kim, S. Y.Cho, K. S. Hong, Investigation of the relations between structure and microwave dielectric properties of divalent metal tungstate compounds, J. Eur. Ceram. Soc. 26 (2006) 2051–2054.

[20] D. Zhou, D. Guo, W. B. Li, L. X. Pang, X. Yao, D. W. Wang, I. M. Reaney, Novel temperature stable high-εr microwave dielectrics in the Bi_2O_3–TiO_2–V_2O_5 system, J. Mater. Chem. C 4 (2016) 5357–5362.

[21] D. Zhou, L. X. Pang, J. Guo, Z. M. Qi, T. Shao, X. Yao, C. A. Randall, Phase evolution, phase transition, and microwave dielectric properties of scheelite structured $xBi(Fe_{1/3}Mo_{2/3})O_4$–$(1-x)BiVO_4$ ($0.0\leq x\leq 1.0$) low temperature firing ceramics, J. Mater. Chem. 22 (2012) 21412–21419.

[22] T. Lu, Electrical conductivity of polycrystalline $BiVO_4$ samples having the scheelite structure, Solid State Ionics 21 (1986) 339–342.

[23] A. W. Sleight, H. Y. Chen, A. Ferretti, D. E. Crystal growth and structure of $BiVO_4$. Mater. Res. Bull. 14 (1979) 1571–1581.

[24] M. Valant, D. Suvorov, Chemical Compatibility between Silver Electrodes and Low-Firing Binary-Oxide Compounds: Conceptual Study, J. Am. Ceram. Soc. 83 (2000) 2721–2729.

[25] S. H. Wee, D. W. Kim, S. I. Yoo, Microwave Dielectric Properties of Low-Fired $ZnNb_2O_6$ Ceramics with $BiVO_4$ Addition, J. Am. Ceram. Soc. 87 (2004) 871–874.

[26] D. Zhou, L. X. Pang, J. Guo, Y. Wu, G. Q. Zhang, H. Wang, X. Yao, Sintering behavior and microwave dielectric properties of novel low temperature firing

$Bi_3FeMo_2O_{12}$ Ceramic, J. Adv. Dielectrics 1 (2011) 379–382.

[27] L. X. Pang, D. Zhou, J. Guo, Z. M. Qi, T. Shao, Microwave dielectric properties of scheelite structured low temperature fired $Bi(In_{1/3}Mo_{2/3})O_4$ ceramic, Ceram. Int. 39 (2013) 4719–4722.

[28] K. Wakino, M. Murata, H. Tamura, Far Infrared Reflection Spectra of Ba(Zn, Ta)O_3-$BaZrO_3$ Dielectric Resonator Material, J. Am. Ceram. Soc. 69 (1986) 34–37.

[29] S. Kamba, H. Wang, M. Berta, F. Kadlec, J. Petzelt, D. Zhou, X. Yao, Correlation between infrared, THz and microwave dielectric properties of vanadium doped antiferroelectric $BiNbO_4$, J. Eur. Ceram. Soc. 26 (2006) 2861–2865.

[30] M. Tonouchi, Cutting-edge terahertz technology, Nature Photon. 1 (2007) 97–105.

[31] L. Duvillaret, F. Garet, J. L. Coutaz, Highly precise determination of optical constants and sample thickness in Terahertz time-domain spectroscopy, Appl. Opt. 38 (1999) 409–415.

[32] S. Nashima, O. Morikawa, K. Takata, M. Hangyo, Temperature dependence of optical and electronic properties of moderately doped silicon at terahertz frequencies, J. Appl. Phys. 90 (2001) 837–842.

[33] J. Krupka,; K. Derzakowski, B. Riddle, J. Baker-Jarvis, A dielectric resonator for measurements of complex permittivity of low loss dielectric materials as a function of temperature, Meas. Sci. Technol. 9 (1998) 1751–1756.

[34] R. D. Shannon, Dielectric polarizabilities of ions in oxides and fluorides, J. Appl. Phys. 73 (1993) 348–366.

[35] P. V. Rysselberghe, Remarks concerning the Clausius–Mossotti Law, J. Phys. Chem. 36 (1932) 1152–1155.

[36] W. B. Li, D. Zhou, H. H. Xi, L. X. Pang, X. Yao, Structure, Infrared Reflectivity

and Microwave Dielectric Properties of $(Na_{0.5}La_{0.5})MoO_4$–$(Na_{0.5}Bi_{0.5})MoO_4$ Ceramics, J. Am. Ceram. Soc. 99 (2016) 2083–2088.

[37] J. Wang, Z. Yue, Z. Gui, L. Li, Low-temperature sintered $Zn(Nb_{1-x}V_{x/2})_2O_{6-2.5x}$ microwave dielectric ceramics with high Q value for LTCC application, J. Alloy. Comp. 392 (2005) 263–267.

[38] S. O. Yoon, J. H. Yoon, K. S. Kim, S. H. Shim, Y. K. Pyeon, Microwave dielectric properties of $LiNb_3O_8$ ceramics with TiO_2 additions, J. Eur. Ceram. Soc. 26 (2006) 2031–2034.

[39] J. X. Tong, Q. L. Zhang, H. Yang, J. L. Zou, Low-temperature firing and microwave dielectric properties of $Ca[(Li_{0.33}Nb_{0.67})_{0.9}Ti_{0.1}]O_{3-\delta}$ ceramics with LiF addition, Mater. Lett. 59 (2005) 3252–3255.

[40] Y. C. Choi, J. H. Park, S. Nahm and J. G. Park, Middle- and high-permittivity dielectric compositions for low-temperature co-fired ceramics, J. Eur. Ceram. Soc. 27 (2007) 2017–2024.

[41] D. Zhou D, W. B. Li, J. Guo, L. X. Pang, Z. M. Qi, T. Shao, H. D. Xie, Z. X. Yue, X. Yao, Structure, Phase Evolution, and Microwave Dielectric Properties of $(Ag_{0.5}Bi_{0.5})(Mo_{0.5}W_{0.5})O_4$ Ceramic with Ultra low Sintering Temperature, Inor. Chem. 53 (2014) 5712–5716.

[42] K. P. Surendran, M. T. Sebastian, P. Mohanan, R. L. Moreira, and A. Dias. Effect of stoichiometry on the microwave dielectric properties of $Ba(Mg_{1/3}Ta_{2/3})O_3$ dielectric ceramics, Chem. Mater. 17 (2005) 142–151.

Table 1. Refined atomic fractional coordinates from XRD data for the $Bi(Sc_{1/3}Mo_{2/3})O_4$ sample and the lattice parameters at room temperature are a = 16.9821(9) Å, b = 11.6097(3) Å, c = 5.3099(3) Å and β = 104.649(2) °. The space group is C12/C 1 (No. 15).

Atom	Site	Occ.	x	y	z	Biso
Bi1	8f	1.0	0.15469	0.88144	0.43115	0.91340
Bi2	4e	0.5	0.00000	0.66245	0.25000	0.77108
Sc1	4e	0.5	0.00000	0.09457	0.25000	1.41238
Mo1	8f	1.0	0.16931	0.37373	0.42545	1.08227
O1	8f	1.0	0.09109	0.02057	0.58513	0.33135
O2	8f	1.0	0.05002	0.21419	0.05169	0.86399
O3	8f	1.0	0.21725	0.29943	0.25622	0.01887
O4	8f	1.0	0.12522	0.29056	0.60635	0.12964
O5	8f	1.0	0.08863	0.45317	0.23918	1.13359
O6	8f	1.0	0.22393	0.45212	0.62496	0.96063

Table 2. Refined cell parameters, reliability factors and bond length data for $Bi(Sc_{1/3}Mo_{2/3})O_4$.

	$Bi(Sc_{1/3}Mo_{2/3})O_4$
a(Å)	16.9821(9)
b(Å)	11.6097(3)
c(Å)	5.3099(3)
β(°)	104.649(2)
R_p	9.03 %
R_{wp}	13.1 %
R_{exp}	12.8 %
S	1.02
Bi(1)-O(Å)	2.1984~2.8952
Bi(2)-O(Å)	2.1565~2.9727
Sc-O(Å)	2.0522~2.373
Mo-O(Å)	1.5212~1.7380

Table 3. Sintering temperatures and microwave dielectric properties of low temperature firing microwave dielectric ceramics with permittivity value around ~ 25

Composition	Sintering Temperature	ε_r	Qf value (GHz)	TCF Value (ppm/^{o}C)	Ref.
$0.45(Na_{0.5}La_{0.5})MoO_4$ –$0.55(Na_{0.5}Bi_{0.5})MoO_4$	640	23.1	17,500	+0.3	36
$Zn(Nb_{1-x}V_{x/2})_2O_{6-2.5x}$ (x=0.15)	975	23.3	37,000	−71	37
$LiNb_3O_8$	1075	24	58,000	−96	38
$Bi(Sc_{1/3}Mo_{2/3})O_4$	930	24.4	48,100	−68	This work
$Ca[(Li_{0.33}Nb_{0.67})_{0.9}Ti_{0.1}]O_{3-\delta}$ +10 wt-%LiF	900	24.8	19,300	−15	39
$Bi(In_{1/3}Mo_{2/3})O_4$	840	25.2	40,000	−65	27
85 wt-%$BaTi_4O_9$ +15wt%Li–B–Si–Ca–Al-O	875	26	10,200	0	40
$(AgBi)(MoW)O_4$	580	26.3	10,000	+20	41
$Bi(Fe_{1/3}Mo_{2/3})O_4$	845	27.2	14,500	−80	26

Table 4. Phonon parameters obtained from the fitting of the infrared reflectivity spectra of the $Bi(Sc_{1/3}Mo_{2/3})O_4$ ceramic

Mode	ω_{oj}	ω_{pj}	γ_j	$\Delta\varepsilon_j$
1	65.383	86.342	4.951	1.74
2	73.143	132.2	7.261	3.27
3	91.994	196.17	8.425	4.55
4	101.8	64.066	6.091	0.396
5	116.66	106.1	9.497	0.827
6	131.83	128.97	12.283	0.957
7	151.33	102.77	12.137	0.461
8	162.4	149.73	20.018	0.85
9	195.12	135.08	16.866	0.479
10	217.77	145.59	15.388	0.447
11	248.95	240.52	22.203	0.933
12	300.96	318.42	35.762	1.12
13	369.75	313.29	43.397	0.718
14	412.1	357.89	46.964	0.754
15	443.37	238.66	35.181	0.29
16	487	120.12	25.678	0.061
17	536.78	121.2	36.073	0.051
18	598.39	247.17	96.098	0.171
19	700.09	451.21	80.296	0.415
20	761.25	204.22	41.374	0.072
21	799.91	140.43	19.264	0.031
22	819.06	82.13	13.825	0.01

23	863.34	71.578	14.908	0.007
24	879.66	55.112	10.582	0.004
	ε_∞=2.72		ε_0=21.334	

Figure Captions:

Fig. 1. Experimental (circles) and calculated (line) XRD profiles for the $Bi(Sc_{1/3}Mo_{2/3})O_4$ sample at room temperature (R_p = 9.03 %, R_{wp} = 13.1 %, R_{exp} = 12.8 % and S = 1.02. The short vertical lines below the patterns mark the positions of Bragg reflections. The bottom continuous line is the difference between the observed and the calculated intensity.) (a), the schematic structure of $Bi(Sc_{1/3}Mo_{2/3})O_4$ (b) and selected area electron diffraction (SAED) patterns and related high resolution imaging (c).

Fig. 2. SEM image of the as-fired (a) and fractured (b) surfaces of $(Sc_{1/3}Mo_{2/3})O_4$ ceramic sintered at 930 ^oC

Fig. 3. Complex impedance plot recorded at 448 and 502 ^oC (The numbers denote the logarithm values of the selected frequencies marked by filled squares) (a), and Arrhenius-type plot of bulk conductivity (b) for the $Bi(Sc_{1/3}Mo_{2/3})O_4$ ceramic sintered 2 h at 930 ^oC

Fig. 4. Microwave dielectric properties of the $Bi(Sc_{1/3}Mo_{2/3})O_4$ ceramics as a function of sintering temperature

Fig. 5. Wideband complex dielectric spectra of the $Bi(Sc_{1/3}Mo_{2/3})O_4$ ceramic in frequency range 20 Hz ~ 30 THz (20 Hz ~ 1 MHz measured by Agilent E4980LCR, 6.84 GHz measured using $TE_{01\delta}$ by network analyzer, 0.1 ~ 1.4 THz (4 ~ 48 cm^{-1}) by THz-TDS transmission spectroscopy, 0.3 GHz ~ 30 THz (0.01 ~ 1000 cm^{-1}) by infrared reflectivity spectroscopy fitting) and room temperature infrared reflectivity spectra (circles are experimental at microwave region and THz data, solid lines represent the fit of IR spectra)

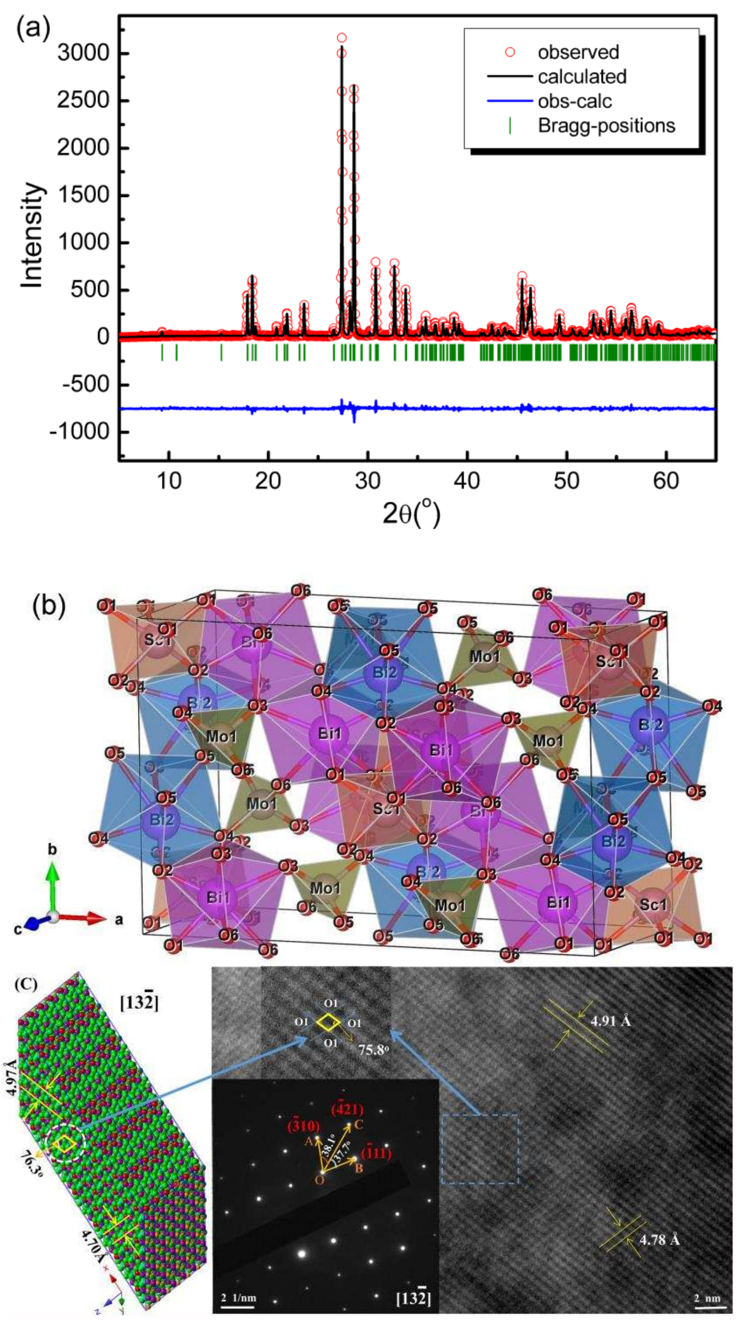

Fig. 1. Experimental (circles) and calculated (line) XRD profiles for the $Bi(Sc_{1/3}Mo_{2/3})O_4$ sample at room temperature (R_p = 9.03 %, R_{wp} = 13.1 %, R_{exp} = 12.8 % and S = 1.02. The short vertical lines below the patterns mark the positions of Bragg reflections. The bottom continuous line is the difference between the observed and the calculated intensity.) (a), the schematic structure of $Bi(Sc_{1/3}Mo_{2/3})O_4$ (b) and selected area electron diffraction (SAED) patterns and related high resolution imaging (c).

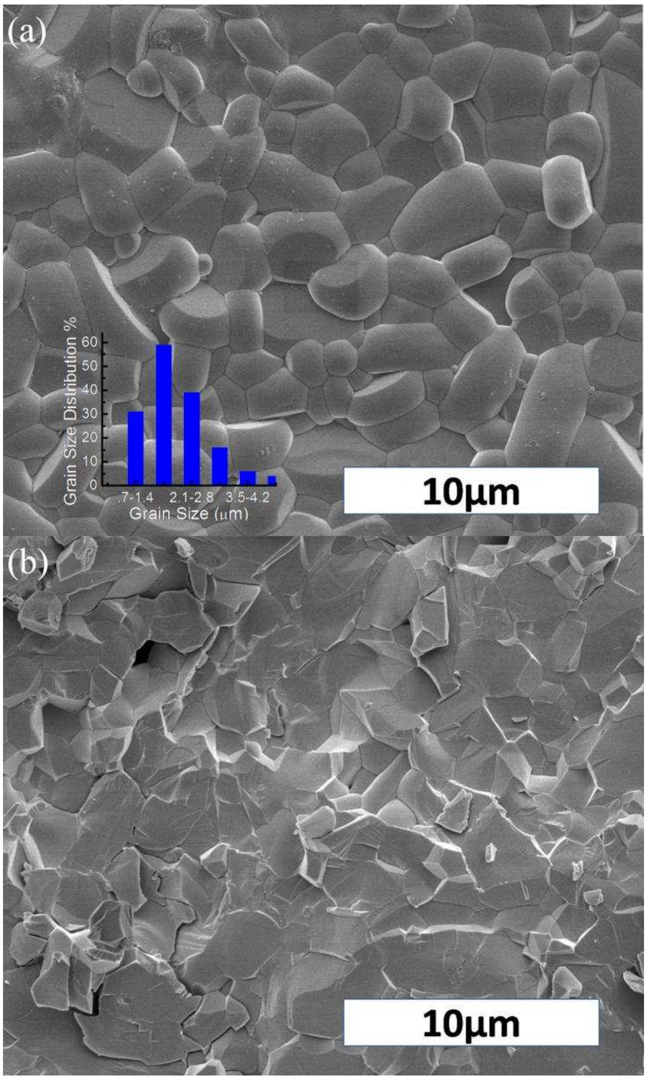

Fig. 2. SEM image of the as-fired (a) and fractured (b) surfaces of $(Sc_{1/3}Mo_{2/3})O_4$ ceramic sintered at 930 ^{o}C

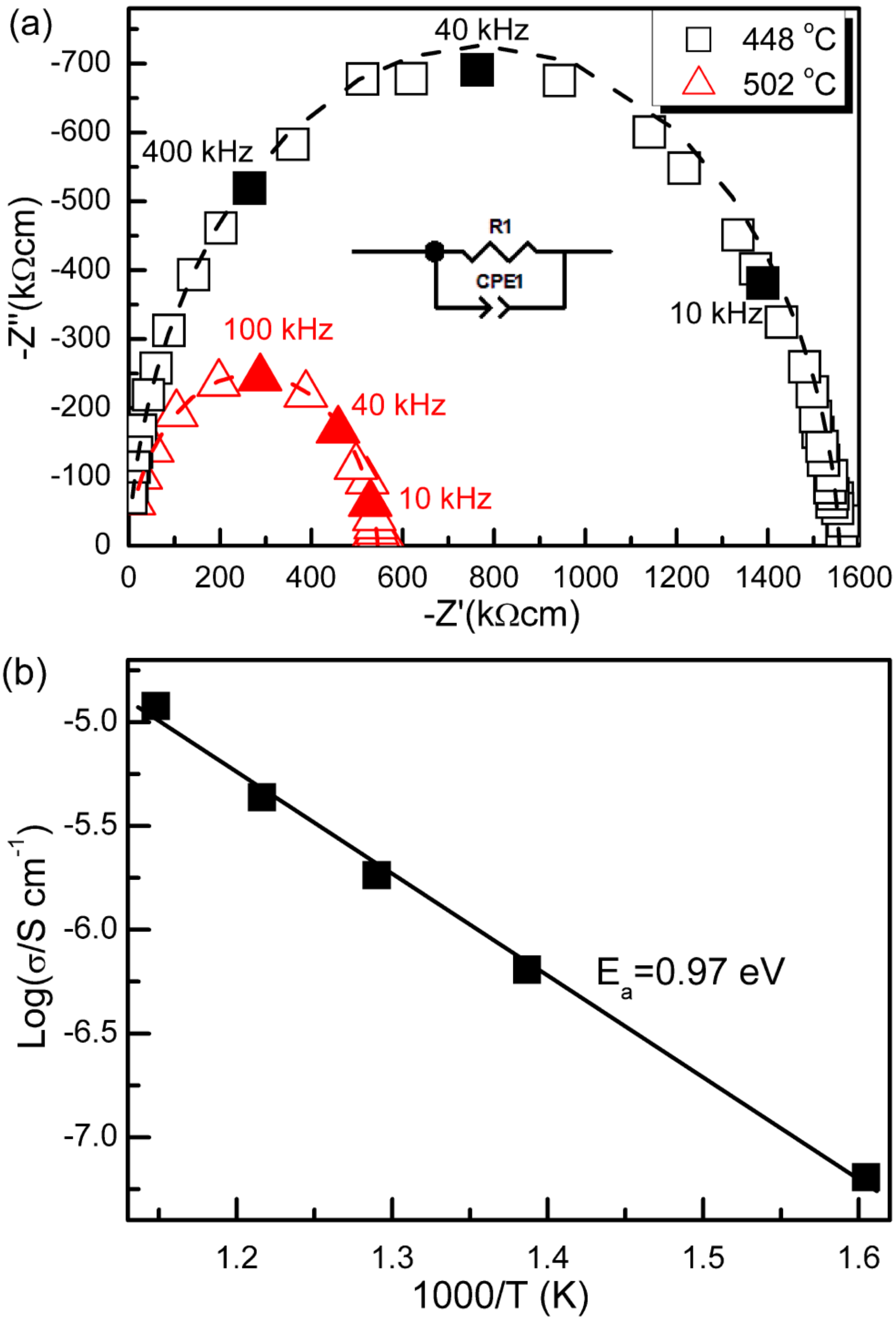

Fig. 3. Complex impedance plot recorded at 448 and 502 °C (The numbers denote the logarithm values of the selected frequencies marked by filled squares) (a), and Arrhenius-type plot of bulk conductivity (b) for the $Bi(Sc_{1/3}Mo_{2/3})O_4$ ceramic sintered 2 h at 930 °C

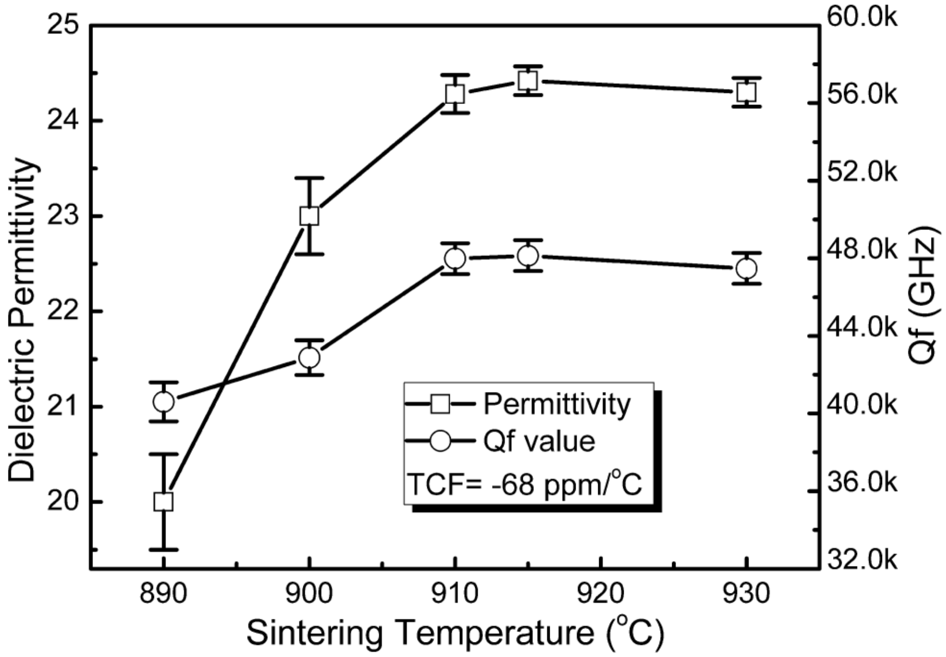

Fig. 4. Microwave dielectric properties of the $Bi(Sc_{1/3}Mo_{2/3})O_4$ ceramics as a function of sintering temperature

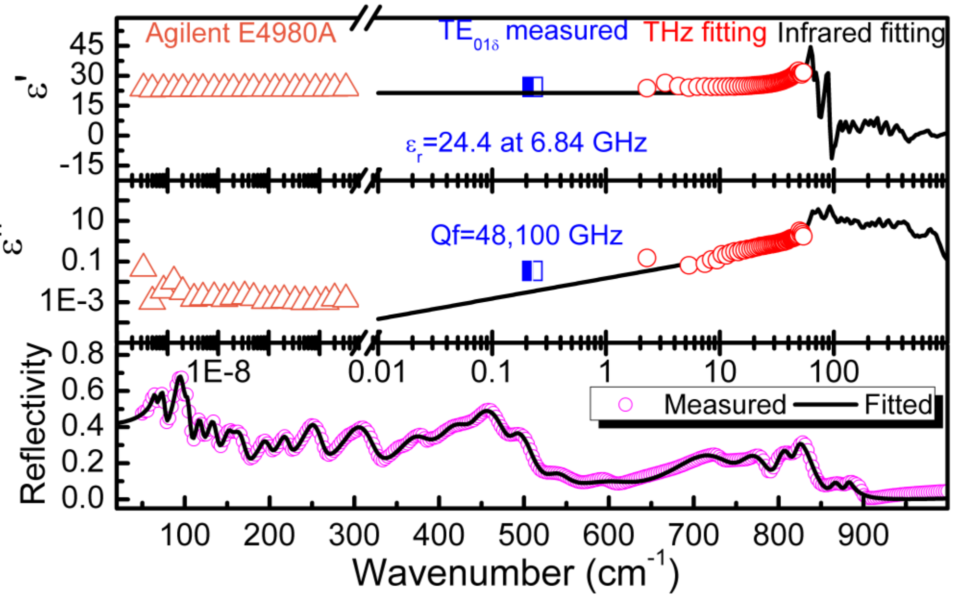

Fig. 5. Wideband complex dielectric spectra of the $Bi(Sc_{1/3}Mo_{2/3})O_4$ ceramic in frequency range 20 Hz ~ 30 THz (20 Hz ~ 1 MHz measured by Agilent E4980LCR, 6.84 GHz measured using $TE_{01\delta}$ by network analyzer, 0.1 ~ 1.4 THz (4 ~ 48 cm^{-1}) by THz-TDS transmission spectroscopy, 0.3 GHz ~ 30 THz (0.01 ~ 1000 cm^{-1}) by infrared reflectivity spectroscopy fitting) and room temperature infrared reflectivity spectra (circles are experimental at microwave region and THz data, solid lines represent the fit of IR spectra)